

## Topological winding guaranteed coherent orthogonal scattering

Cheng Guo<sup>\*</sup> and Shanhui Fan<sup>†</sup>

Ginzton Laboratory and Department of Electrical Engineering, Stanford University, Stanford, California 94305, USA



(Received 2 November 2023; revised 25 April 2024; accepted 10 June 2024; published 27 June 2024)

Coherent control has enabled various novel phenomena in wave scattering. We introduce an effect called coherent orthogonal scattering, where the output wave becomes orthogonal to the reference output state without scatterers. This effect leads to a unity extinction coefficient and complete mode conversion. We examine the conditions for this effect and reveal its topological nature by relating it to the indivisibility between the dimension and the winding number of scattering submatrices. These findings deepen our understanding of topological scattering phenomena.

DOI: 10.1103/PhysRevA.109.L061503

Understanding wave scattering is crucial for various applications, such as imaging [1–12], sensing [13,14], energy harvesting [15–31], and optical computing [32–36]. Coherent control of wave scattering [37–39] has been a significant advancement, enabling the tailoring of scattering behaviors by modifying the input wave profile. This approach has unveiled unique phenomena, particularly coherent perfect absorption [40–49]—the complete absorption of a tailored input wave profile—and related effects [50–52], including coherent virtual absorption [53–55] and reflectionless scattering modes [56–59].

In this Letter we introduce a phenomenon called *coherent orthogonal scattering*, which refers to the complete extinction of the output state with respect to the reference output state in the absence of scatterers. Consider a standard scattering setup [60,61]. Let  $H$  be the Hilbert space of waves. We input a normalized state  $|\psi\rangle$  into a system. In the absence of scatterers [Fig. 1(a)], the output state, termed the reference state, is

$$|\xi_0\rangle = \hat{S}_0|\psi\rangle, \quad (1)$$

where  $\hat{S}_0$  is a unitary background scattering operator. In the presence of scatterers [Fig. 1(b)], the output state is

$$|\xi\rangle = \hat{S}|\psi\rangle, \quad (2)$$

where  $\hat{S}$  is the total scattering operator, which can be nonunitary. By orthogonal projection with respect to  $|\xi_0\rangle$ , the output state  $|\xi\rangle$  can be uniquely decomposed as

$$|\xi\rangle = \alpha|\xi_0\rangle + \beta|\xi_0^\perp\rangle, \quad (3)$$

where  $|\xi_0^\perp\rangle$  is a unit vector orthogonal to  $|\xi_0\rangle$ . The absorption coefficient is defined as

$$\chi_a = 1 - |\alpha|^2 - |\beta|^2 = 1 - \langle\psi|\hat{S}^\dagger\hat{S}|\psi\rangle. \quad (4)$$

The extinction coefficient is defined as

$$\chi_e = 1 - |\alpha|^2 = 1 - |\langle\xi_0|\xi\rangle|^2 = 1 - |\langle\psi|\hat{S}_0^\dagger\hat{S}|\psi\rangle|^2, \quad (5)$$

which measures the deviation of  $|\xi\rangle$  from  $|\xi_0\rangle$  [62]. For passive scatterers,  $\chi_a$  and  $\chi_e$  lie between 0 and 1.

In coherent control experiments, one varies  $|\psi\rangle$  within an accessible input subspace  $H_i \subseteq H$  to achieve desired outcomes [63–65]. Coherent perfect absorption refers to the case when  $\chi_a = 1$ . In contrast, coherent orthogonal scattering occurs when  $\chi_e = 1$ , which is equivalent to the output state being orthogonal to the reference state:

$$\langle\xi_0|\xi\rangle = \langle\psi|\hat{S}_0^\dagger\hat{S}|\psi\rangle = 0. \quad (6)$$

For example, in polarization optics,  $H_i$  is the two-dimensional (2D) polarization space, and the coherent orthogonal scattering corresponds to complete polarization conversion [Fig. 1(c)]. A related yet distinct effect, coherent perfect extinction [52], refers to the case when the output state is orthogonal to the reference output subspace  $H_o = \hat{S}_0H_i$ :

$$\forall|\phi\rangle \in H_i, \quad \langle\phi|\hat{S}_0^\dagger\hat{S}|\psi\rangle = 0. \quad (7)$$

We can express Eqs. (6) and (7) in matrix forms. Suppose  $H_i$  is  $m$  dimensional. Using a set of orthonormal bases, the compression of  $\hat{S}_0^\dagger\hat{S}$  to  $H_i$  is represented by an  $m \times m$  scattering submatrix  $\tilde{S}$  [66]. (In the absence of scatterers,  $\hat{S} = \hat{S}_0$ , thus  $\tilde{S} = I$ .) Then Eq. (6) becomes

$$\exists \tilde{\mathbf{a}} \in \mathbb{C}^m \setminus \{\mathbf{0}\}, \quad \tilde{\mathbf{a}}^\dagger \tilde{S} \tilde{\mathbf{a}} = 0, \quad (8)$$

while Eq. (7) becomes

$$\exists \tilde{\mathbf{a}} \in \mathbb{C}^m \setminus \{\mathbf{0}\}, \quad \tilde{S} \tilde{\mathbf{a}} = \mathbf{0}. \quad (9)$$

The physical significance of coherent orthogonal scattering is twofold. First, it corresponds to a unity extinction coefficient, a fundamental observable in scattering experiments with applications in diverse areas, including molecular spectroscopy [67–70], acoustic imaging [71], atmospheric science [72,73], and astronomy [50,74]. Understanding the conditions for achieving a unity extinction coefficient is important. Second, coherent orthogonal scattering enables complete mode conversion [75–82], such as complete polarization conversion [83–95], which plays a crucial role in various applications, including communications [79,96–98], sensing [99–103], and

\*Contact author: guocheng@stanford.edu

<sup>†</sup>Contact author: shanhui@stanford.edu

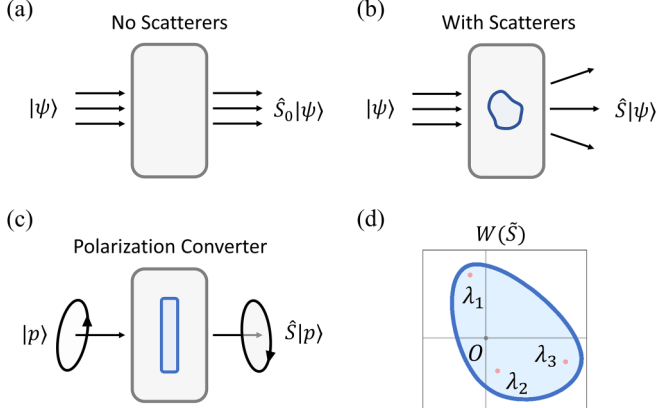


FIG. 1. The concept of coherent orthogonal scattering (COS). (a), (b) A standard scattering setup with an input state  $|\psi\rangle$ . (a) In the absence of scatterers, the output state is  $|\xi_0\rangle = \hat{S}_0|\psi\rangle$ . (b) In the presence of scatterers, the output state becomes  $|\xi\rangle = \hat{S}|\psi\rangle$ . COS occurs when  $\langle \xi_0 | \xi \rangle = 0$ . (c) In polarization optics, COS corresponds to complete polarization conversion. (d) The numerical range  $W(\tilde{S})$  of a scattering submatrix  $\tilde{S}$  is convex and contains its eigenvalues. COS occurs iff  $0 \in W(\tilde{S})$ .

quantum technology [104–107]. A key challenge in mode converter design is determining whether complete mode conversion can be achieved by adjusting specific design parameters and efficiently identifying the parameter values that result in complete mode conversion [84,91,97,108]. This again requires a deeper understanding of the conditions for coherent orthogonal scattering.

In this work we investigate the conditions for coherent orthogonal scattering. A useful mathematical concept for this purpose is the *numerical range* of  $\tilde{S}$  [109,110]:

$$W(\tilde{S}) := \{x^\dagger \tilde{S} x : x \in \mathbb{C}^m, x^\dagger x = 1\}. \quad (10)$$

$W(\tilde{S})$  is a compact *convex* subset of  $\mathbb{C}$  that contains all the eigenvalues of  $\tilde{S}$  [111,112]. (See Supplemental Material (SM) [113], Sec. I, for more details.) Figure 1(d) shows  $W(\tilde{S})$  for an  $\tilde{S} \in M_3$ . The *Crawford number* of  $\tilde{S}$  is the distance of  $W(\tilde{S})$  from the origin [114–116]:

$$c(\tilde{S}) := \min\{|z| : z \in W(\tilde{S})\}. \quad (11)$$

From Eq. (8), coherent orthogonal scattering occurs iff

$$0 \in W(\tilde{S}), \quad \text{i.e.,} \quad c(\tilde{S}) = 0. \quad (12)$$

The condition (12) can be numerically checked using an approximate algorithm [109] (see SM, Sec. I D), but it cannot be determined analytically using the entries of  $\tilde{S}$  when  $m \geq 4$  [117,118]. In contrast, coherent perfect extinction occurs iff [52]

$$\det \tilde{S} = 0, \quad (13)$$

which can be easily checked using the entries of  $\tilde{S}$  [119]. Hence, the key challenge is to find a simple analytical criterion for coherent orthogonal scattering.

Here, we present a simple sufficient analytical criterion for coherent orthogonal scattering. Our idea is to examine not a single, but a *loop* of scattering submatrices [Fig. 2(a)].

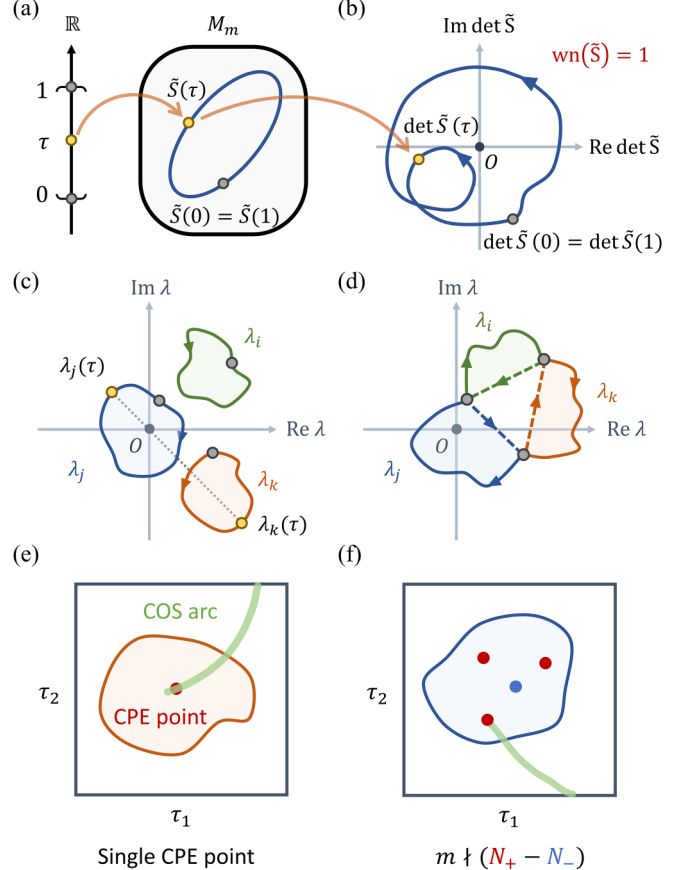


FIG. 2. Topological winding guaranteed coherent orthogonal scattering. (a) A loop of  $\tilde{S}(\tau) \in M_m$ . (b)  $\det \tilde{S}(\tau)$  has a winding number  $\text{wn}(\tilde{S})$ . If  $m$  does not divide  $\text{wn}(\tilde{S})$ , denoted as  $m \nmid \text{wn}(\tilde{S})$ , coherent orthogonal scattering must occur for some  $\tilde{S}(\tau_0)$ . (c), (d) The path of eigenvalues when (c)  $v(\tilde{S}) = \text{id}$ , (d)  $v(\tilde{S}) \neq \text{id}$ . (e), (f) CPE points and COS arcs in a 2D parameter space. (e) A topological COS arc exists associated with each CPE point. (f) A topological COS arc exists across a simple loop that surrounds multiple CPE points if  $m \nmid (N_+ - N_-)$ . COS arcs within the loop are not shown.

Consider a continuous map

$$\tilde{S} : [0, 1] \rightarrow M_m, \quad \tau \mapsto \tilde{S}(\tau), \quad (14)$$

where  $\tilde{S}(0) = \tilde{S}(1)$ . We ask whether

$$\exists \tau_0 \in [0, 1], \quad 0 \in W[\tilde{S}(\tau_0)], \quad (15)$$

motivated by the question of whether coherent orthogonal scattering can be achieved by tuning a certain parameter.

Our criterion is as follows. We calculate  $\det \tilde{S}(\tau)$  and check whether

$$\exists \tau_0 \in [0, 1], \quad \det \tilde{S}(\tau_0) = 0. \quad (16)$$

If true, then  $\tilde{S}(\tau_0)$  exhibits coherent perfect extinction, and thus also coherent orthogonal scattering. If false, then  $\det \tilde{S}$  traces a closed path in  $\mathbb{C} \setminus \{0\}$  [Fig. 2(b)], which has a well-defined winding number around the origin [52,120]:

$$\text{wn}(\tilde{S}) := \varphi(1) - \varphi(0) \in \mathbb{Z}, \quad (17)$$

where  $2\pi\varphi(\tau)$  is the continuous polar angle of  $\det \tilde{S}(\tau)$ . If  $m$  does not divide  $\text{wn}(\tilde{S})$ , denoted as  $m \nmid \text{wn}(\tilde{S})$ , then

$$\exists \tau_0 \in [0, 1], \quad 0 \in W[\tilde{S}(\tau_0)]. \quad (18)$$

If  $m$  divides  $\text{wn}(\tilde{S})$ , denoted as  $m \mid \text{wn}(\tilde{S})$  [121], such  $\tau_0$  may or may not exist. See SM, Sec. II for examples.

The criterion (18) is our main result. It can be proved using a theorem established in Refs. [122,123]. Here, we outline the essential ideas. Consider the  $m$  eigenvalues of  $\tilde{S}(\tau)$ , denoted as  $\lambda_1(\tau), \dots, \lambda_m(\tau)$ . Since  $\tilde{S}(\tau)$  is a continuous map from  $[0,1]$  to  $\text{GL}_n$ , we can choose all  $\lambda_j(\tau)$ 's to be continuous functions from  $[0,1]$  to  $\mathbb{C} \setminus \{0\}$  [124,125] (see SM, Sec. III). Since  $\tilde{S}(0) = \tilde{S}(1)$ , the set of  $\lambda_j(1)$ 's must coincide with the  $\lambda_j(0)$ 's, up to a permutation

$$\lambda_j(1) = \lambda_{v_j}(0); \quad v(\tilde{S}) = \begin{pmatrix} 1 & 2 & \dots & m \\ v_1 & v_2 & \dots & v_m \end{pmatrix}. \quad (19)$$

For simplicity, let us first consider the special case when the permutation is the identity [ $v(\tilde{S}) = \text{id}$ ]. Then, each  $\lambda_j(\tau)$  traces out a loop in the punctuated complex plane with a well-defined winding number about the origin:

$$\text{wn}(\lambda_j) \in \mathbb{Z}, \quad j = 1, \dots, m. \quad (20)$$

There is a simple yet important relation,

$$\text{wn}(\tilde{S}) = \sum_{j=1}^m \text{wn}(\lambda_j), \quad (21)$$

which follows from the fact that [120]

$$\det \tilde{S}(\tau) = \prod_{i=1}^m \lambda_i(\tau). \quad (22)$$

Combining Eq. (21) with our premise  $m \nmid \text{wn}(\tilde{S})$ , there must exist a pair of eigenvalue loops, say  $\lambda_j$  and  $\lambda_k$ , that have different winding numbers. As  $\tau$  runs over  $[0,1]$ , the line segment  $\overline{\lambda_j(\tau)\lambda_k(\tau)}$  connecting these two eigenvalues must sweep across the origin at least once, implying that

$$\exists \tau_0 \in [0, 1], \quad 0 \in \overline{\lambda_j(\tau_0)\lambda_k(\tau_0)} \subseteq W[\tilde{S}(\tau_0)]. \quad (23)$$

Here we used the fact that the numerical range contains the convex hull of the eigenvalues [111,112]. This completes the proof for the  $v(\tilde{S}) = \text{id}$  case. To prove the  $v(\tilde{S}) \neq \text{id}$  cases [Fig. 2(d)], we construct  $\tilde{S}' : [0, 1] \rightarrow \text{GL}_m$ , which undoes the permutation  $v(\tilde{S})$  along the line segments  $\overline{\lambda_{v_j}(0)\lambda_j(0)}$ . The concatenation of  $\tilde{S}$  and  $\tilde{S}'$  becomes a loop with the identity permutation, allowing the previous analysis to complete the proof [123].

With the mathematical groundwork established, we now discuss the physical implications of criterion (18). First, our criterion establishes a deeper connection between coherent orthogonal scattering and coherent perfect extinction. Consider an  $\tilde{S} \in M_m$  with  $m \geq 2$  that depends continuously on two parameters  $\tau = (\tau_1, \tau_2) \in \Omega$ , where  $\Omega$  is a compact and simply connected subset of  $\mathbb{R}^2$ . Coherent perfect extinction generically occurs in  $\Omega$  at isolated points, known as CPE points [52]. Along a simple closed curve that encloses a single generic CPE point [Fig. 2(e)],

$$\text{wn}(\tilde{S}) = \pm 1. \quad (24)$$

Since  $m \nmid \pm 1$ , according to (18), coherent orthogonal scattering must occur somewhere along the loop. We can deform the loop continuously and deduce that coherent orthogonal scattering must occur along at least one arc, referred to as a COS arc. Such a COS arc is topologically protected. We can extend this analysis to the case of multiple CPE points [Fig. 2(f)]. Suppose there are  $N_+$  and  $N_-$  CPE points with winding numbers  $+1$  and  $-1$ , respectively, enclosed by a simple closed curve. A COS arc must exist across the loop if

$$m \nmid (N_+ - N_-). \quad (25)$$

Second, we investigate the topological winding of scattering submatrices due to a resonance. We consider a single-resonance scattering submatrix [126–128],

$$\tilde{S}(\omega) = \tilde{C} + \frac{\tilde{d}\tilde{\kappa}^T}{-i(\omega - \omega_0) + \gamma} \in M_m, \quad (26)$$

where  $\omega_0$  and  $\gamma$  are the resonant frequency and decay rate, respectively. The column vectors  $\tilde{\kappa}$  and  $\tilde{d}$  represent the coupling rates between the resonator and the input and output waves in the ports, respectively.  $\tilde{C} \in M_m$  describes the background scattering. We can prove that  $\det \tilde{S}(\omega)$  traces out a circle in the complex plane with

$$\text{wn}(\tilde{S}) = \begin{cases} 0, & \text{Re } \tilde{\rho} < \frac{1}{2}, \\ 1, & \text{Re } \tilde{\rho} > \frac{1}{2} \end{cases}, \quad \tilde{\rho} := -\frac{\tilde{\kappa}^T \tilde{C}^{-1} \tilde{d}}{2\gamma} \in \mathbb{C}. \quad (27)$$

When  $\text{Re } \tilde{\rho} = \frac{1}{2}$ , the circle passes through the origin and  $\text{wn}(\tilde{S})$  is undefined. (See the proof in SM, Secs. IV–VI.) Combining (27) and (18), we conclude that when  $m \geq 2$ ,

$$\text{Re } \tilde{\rho} \geq \frac{1}{2} \Rightarrow \exists \omega_c \in (-\infty, \infty), \quad 0 \in W[\tilde{S}(\omega_c)]. \quad (28)$$

We illustrate our theory with two numerical examples. In both cases, coherent orthogonal scattering corresponds to complete polarization conversion in the transmission. The effect of coherent orthogonal scattering can also be demonstrated in other (e.g., spatial) degrees of freedom. Our theoretical analysis applies to these cases as well.

The first example is a one-dimensional dielectric grating taken from Ref. [129]. The structure has a periodicity  $a$ . Each unit cell has a central rod of width  $w = 0.45a$  and height  $h = 1.5a$  with a dielectric constant  $\epsilon_0 = 2.1025$ , and two additional pieces of width  $(a-w)/2 = 0.275a$  and height  $h_d = 0.1a$  with a dielectric constant  $\epsilon_d = 1.21$  [Fig. 3(a)]. This grating supports a band of  $p$ -polarized guided resonances near  $\omega = 0.8 \times 2\pi c/a$  [Fig. 3(b)]. We consider an incident plane wave with an incident angle  $\theta = \pm 5^\circ$ , and calculate the  $2 \times 2$  transmission matrix,

$$\tilde{S}(\omega) = \begin{pmatrix} t_{pp} & 0 \\ 0 & t_{ss} \end{pmatrix}, \quad (29)$$

which is diagonal due to the  $xz$  mirror symmetry. Consequently, we have  $\lambda_1 = t_{pp}$ ,  $\lambda_2 = t_{ss}$ ,  $\det \tilde{S} = t_{pp}t_{ss}$ , and  $W(\tilde{S})$  is the line segment connecting  $t_{pp}$  and  $t_{ss}$ .

Figures 3(c), 3(e), and 3(g) present the results for  $\theta = -5^\circ$ . Figure 3(c) shows that  $|t_{pp}(\omega)|$  exhibits a single

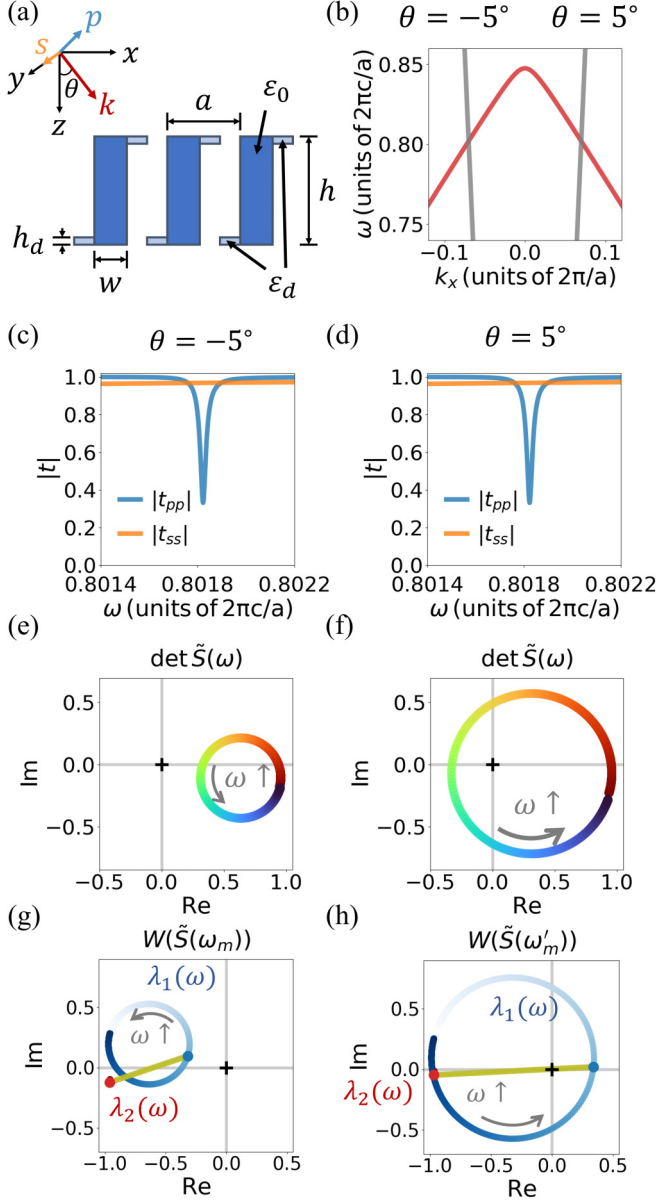


FIG. 3. A grating example. (a) Geometry. (b) Band structure. (c), (e), (g) Results for  $\theta = -5^\circ$ . (c)  $|t_{pp}|(\omega)$  and  $|t_{ss}|(\omega)$ . (e)  $\det \tilde{S}(\omega)$ . (g) Trajectories of  $\lambda_1(\omega)$  and  $\lambda_2(\omega)$ . The red and blue dots denote  $\lambda_1(\omega_m)$  and  $\lambda_2(\omega_m)$ , respectively. The line segment denotes  $W(\tilde{S})$  at  $\omega_m = 0.80182 \times 2\pi c/a$ . (d), (f), (h) Corresponding results for  $\theta = 5^\circ$ . In (h),  $\omega'_m = 0.80220 \times 2\pi c/a$ .

guided resonance [130], while  $|t_{ss}(\omega)|$  almost remains constant. We fit the complex spectra with Eq. (26) and obtain  $\tilde{\rho} = 0.334 - 0.009i$ . Since  $\text{Re } \tilde{\rho} < \frac{1}{2}$ , Eq. (27) predicts that  $\text{wn}(\tilde{S}) = 0$ . Indeed, Fig. 3(e) shows that  $\det \tilde{S}(\omega)$  traces out a circle that does not enclose the origin. Figure 3(g) shows that  $\lambda_1(\omega)$  forms a circle that does not enclose the origin, while  $\lambda_2(\omega)$  almost remains constant. Figure 3(g) also depicts  $W(\tilde{S})$  at  $\omega_m = 0.80182 \times 2\pi c/a$ , where  $c(\tilde{S})$  reaches minimum.  $W[\tilde{S}(\omega_m)]$  forms a line segment connecting  $\lambda_1(\omega_m)$  and  $\lambda_2(\omega_m)$  with  $0 \notin W[\tilde{S}(\omega_m)]$ . Thus, coherent orthogonal scattering does not occur in the entire frequency range.

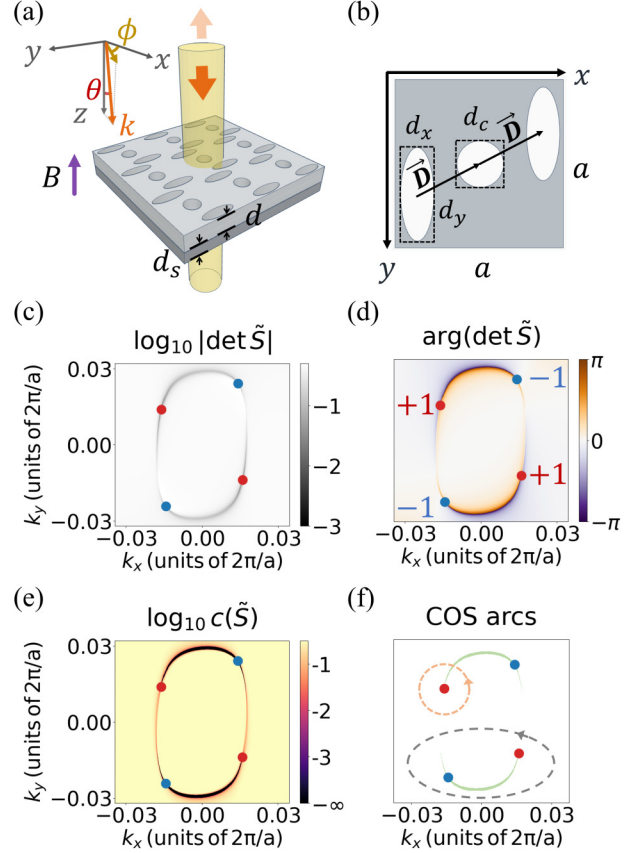


FIG. 4. A photonic crystal slab example. (a) Geometry. (b) Unit cell. (c)–(f) Results for  $\tilde{S}(k_x, k_y)$  at  $\omega = 0.386 \times 2\pi c/a$ . (c)  $\log_{10} |\det \tilde{S}(k_x, k_y)|$ . (d)  $\arg[\det \tilde{S}(k_x, k_y)]$ . (e)  $\log_{10} c(\tilde{S})$ . (f) The green region: the COS arcs. The red and blue dots: CPE points with winding numbers +1 and -1, respectively.

Figures 3(d), 3(f), and 3(h) present the results for  $\theta = 5^\circ$ . The transmission amplitude spectra in Fig. 3(d) are similar to those in Fig. 3(c); the differences are in the phases. We fit the complex spectra and obtain  $\tilde{\rho} = 0.666 - 0.009i$ . Since  $\text{Re } \tilde{\rho} > \frac{1}{2}$ , Eq. (27) states that  $\text{wn}(\tilde{S}) = 1$ , and (28) predicts that coherent orthogonal scattering must occur at some frequency. Indeed, Fig. 3(f) shows that  $\det \tilde{S}(\omega)$  traces out a circle that winds around the origin once counterclockwise. Figure 3(h) shows that  $\lambda_1(\omega)$  winds around the origin once, while  $\lambda_2(\omega)$  almost remains constant. Figure 3(h) depicts  $W(\tilde{S})$  at  $\omega'_m = 0.80220 \times 2\pi c/a$ , which is the line segment connecting  $\lambda_1(\omega'_m)$  and  $\lambda_2(\omega'_m)$  with  $0 \in W[\tilde{S}(\omega'_m)]$ . Explicit calculation shows that coherent orthogonal scattering occurs at  $\omega'_m$  for the incident polarization  $(0.86\hat{p} + 0.51e^{i\eta}\hat{s})$  with  $\eta$  an arbitrary phase.

The second example is a 2D magneto-optical photonic crystal slab. The structure consists of two layers [Fig. 4(a)]. The first layer is a photonic crystal slab with a lattice constant  $a$  and a thickness  $d = 0.3a$ . It has a square lattice, with each unit cell having a circular hole at the center with a diameter  $d_c = 0.28a$  and two elliptical holes displaced by  $\pm \vec{D} = \pm(0.375a, -0.18a)$  from the center, where the major axis is  $d_y = 0.56a$  and the minor axis is  $d_x = 0.20a$  [Fig. 4(b)]. The second layer is a uniform slab with a thickness  $d_s = 0.2a$ .

Both slabs are made of a magneto-optical material with a relative permittivity tensor,

$$\boldsymbol{\varepsilon} = \begin{pmatrix} \varepsilon_r & i\varepsilon_a & 0 \\ -i\varepsilon_a & \varepsilon_r & 0 \\ 0 & 0 & \varepsilon_r \end{pmatrix}, \quad (30)$$

where  $\varepsilon_r = 12.0$ ,  $\varepsilon_a = 5.0$ . We consider a plane wave with a fixed frequency  $\omega = 0.386 \times 2\pi c/a$  incident from the top side and calculate the  $2 \times 2$  transmission matrix,

$$\tilde{S}(k_x, k_y) = \begin{pmatrix} t_{xx} & t_{xy} \\ t_{yx} & t_{yy} \end{pmatrix}, \quad (31)$$

where  $(k_x, k_y)$  are the transverse wave-vector components. Unlike that in Eq. (29), here  $\tilde{S}$  is a generic  $2 \times 2$  matrix. In general,  $W(\tilde{S})$  forms an elliptical disk with foci at  $\lambda_1$  and  $\lambda_2$  (see SM, Sec. I C).

Figure 4(c) plots

$$\log_{10} |\det \tilde{S}(k_x, k_y)|, \quad (32)$$

which exhibits sharp variations near the isofrequency contour of the guided resonances. There are four CPE points where  $\det \tilde{S} = 0$ . Figure 4(d) shows that  $\det \tilde{S}(k_x, k_y)$  exhibits a  $2\pi$  ( $-2\pi$ ) phase winding around each red (blue) CPE point, indicating a winding number of  $+1$  ( $-1$ ). The two red (blue) CPE points are related by the  $C_2$  symmetry. Figures 4(e) and 4(f) show that  $c[S(k_x, k_y)] = 0$  occurs in two disjoint COS arcs. Each COS arc occupies a two-dimensional domain that contains one red and one blue CPE point in its interior. These COS arcs are topologically protected. For instance,

the orange loop encircles a single CPE point, so there must exist a COS arc that intersects the orange loop. In contrast, the gray loop encircles two CPE points with a total winding number  $N_+ - N_- = 1 - 1 = 0$ . Since  $2 \nmid 0$ , a COS arc may or may not cross the gray loop. Indeed, in this case, the COS arc is contained entirely inside the loop. (See SM, Sec. VII for additional numerical results.) These numerical examples confirm our theoretical predictions.

In conclusion, we have introduced the phenomenon of coherent orthogonal scattering, which occurs when the output wave becomes orthogonal to the reference output state in the absence of scatterers. This effect leads to a unity extinction coefficient and complete mode conversion. We have revealed the topological nature of this effect by establishing a connection between the winding number of scattering submatrices and the existence of coherent orthogonal scattering. We have discovered topologically protected coherent orthogonal scattering arcs in a two-dimensional parameter space, which connect coherent perfect extinction points with opposite winding numbers. These findings provide a deeper understanding of the interplay between topology and scattering phenomena, paving the way for novel approaches to manipulate coherent wave interactions in various physical systems.

This work is funded by a Simons Investigator in Physics grant from the Simons Foundation (Grant No. 827065), by a Multidisciplinary University Research Initiative (MURI) grant from the US Office of Naval Research (Grant No. N00014-20-1-2450), and by the US Department of Energy (Grant No. DE-FG02-07ER46426).

- 
- [1] S. Feng, C. Kane, P. A. Lee, and A. D. Stone, Correlations and fluctuations of coherent wave transmission through disordered media, *Phys. Rev. Lett.* **61**, 834 (1988).
  - [2] I. M. Vellekoop and A. P. Mosk, Focusing coherent light through opaque strongly scattering media, *Opt. Lett.* **32**, 2309 (2007).
  - [3] S. M. Popoff, G. Lerosey, R. Carminati, M. Fink, A. C. Boccara, and S. Gigan, Measuring the transmission matrix in optics: An approach to the study and control of light propagation in disordered media, *Phys. Rev. Lett.* **104**, 100601 (2010).
  - [4] S. Popoff, G. Lerosey, M. Fink, A. C. Boccara, and S. Gigan, Image transmission through an opaque material, *Nat. Commun.* **1**, 81 (2010).
  - [5] I. M. Vellekoop, A. Lagendijk, and A. P. Mosk, Exploiting disorder for perfect focusing, *Nat. Photon.* **4**, 320 (2010).
  - [6] Y. Choi, T. D. Yang, C. Fang-Yen, P. Kang, K. J. Lee, R. R. Dasari, M. S. Feld, and W. Choi, Overcoming the diffraction limit using multiple light scattering in a highly disordered medium, *Phys. Rev. Lett.* **107**, 023902 (2011).
  - [7] S. M. Popoff, G. Lerosey, M. Fink, A. C. Boccara, and S. Gigan, Controlling light through optical disordered media: Transmission matrix approach, *New J. Phys.* **13**, 123021 (2011).
  - [8] J. Bertolotti, E. G. van Putten, C. Blum, A. Lagendijk, W. L. Vos, and A. P. Mosk, Non-invasive imaging through opaque scattering layers, *Nature (London)* **491**, 232 (2012).
  - [9] A. P. Mosk, A. Lagendijk, G. Lerosey, and M. Fink, Controlling waves in space and time for imaging and focusing in complex media, *Nat. Photon.* **6**, 283 (2012).
  - [10] T. Chaigne, O. Katz, A. C. Boccara, M. Fink, E. Bossy, and S. Gigan, Controlling light in scattering media non-invasively using the photoacoustic transmission matrix, *Nat. Photon.* **8**, 58 (2014).
  - [11] O. Katz, P. Heidmann, M. Fink, and S. Gigan, Non-invasive single-shot imaging through scattering layers and around corners via speckle correlations, *Nat. Photon.* **8**, 784 (2014).
  - [12] M. Kim, W. Choi, Y. Choi, C. Yoon, and W. Choi, Transmission matrix of a scattering medium and its applications in biophotonics, *Opt. Express* **23**, 12648 (2015).
  - [13] A. V. Muraviev, V. O. Smolski, Z. E. Loparo, and K. L. Vodopyanov, Massively parallel sensing of trace molecules and their isotopologues with broadband subharmonic mid-infrared frequency combs, *Nat. Photon.* **12**, 209 (2018).
  - [14] X. Tan, H. Zhang, J. Li, H. Wan, Q. Guo, H. Zhu, H. Liu, and F. Yi, Non-dispersive infrared multi-gas sensing via nanoantenna integrated narrowband detectors, *Nat. Commun.* **11**, 5245 (2020).
  - [15] G. Chen, *Nanoscale Energy Transport and Conversion: A Parallel Treatment of Electrons, Molecules, Phonons, and Photons* (Oxford University Press, Oxford, 2005).
  - [16] Z. M. Zhang, *Nano/Microscale Heat Transfer* (McGraw-Hill, New York, 2007).

- [17] J. R. Howell, M. P. Mengüç, and R. Siegel, *Thermal Radiation Heat Transfer*, 6th ed. (CRC Press, London, 2016).
- [18] S. Fan, Thermal photonics and energy applications, *Joule* **1**, 264 (2017).
- [19] J. C. Cuevas and F. J. García-Vidal, Radiative heat transfer, *ACS Photon.* **5**, 3896 (2018).
- [20] R. S. Ottens, V. Quetschke, S. Wise, A. A. Alemi, R. Lundock, G. Mueller, D. H. Reitze, D. B. Tanner, and B. F. Whiting, Near-field radiative heat transfer between macroscopic planar surfaces, *Phys. Rev. Lett.* **107**, 014301 (2011).
- [21] A. P. Raman, M. A. Anoma, L. Zhu, E. Rephaeli, and S. Fan, Passive radiative cooling below ambient air temperature under direct sunlight, *Nature (London)* **515**, 540 (2014).
- [22] S. V. Boriskina, M. A. Green, K. Catchpole, E. Yablonovitch, M. C. Beard, Y. Okada, S. Lany, T. Gershon, A. Zakutayev, M. H. Tahersima, V. J. Sorger, M. J. Naughton, K. Kempa, M. Dagenais, Y. Yao, L. Xu, X. Sheng, N. D. Bronstein, J. A. Rogers, A. P. Alivisatos *et al.*, Roadmap on optical energy conversion, *J. Opt.* **18**, 073004 (2016).
- [23] *Nanotechnology for Energy Sustainability*, edited by B. Raj, M. H. van de Voorde, and Y. R. Mahajan (Wiley-VCH, Weinheim, 2017), Vol. 3.
- [24] A. Fiorino, L. Zhu, D. Thompson, R. Mittapally, P. Reddy, and E. Meyhofer, Nanogap near-field thermophotovoltaics, *Nat. Nanotechnol.* **13**, 806 (2018).
- [25] Y. Park, V. S. Asadchy, B. Zhao, C. Guo, J. Wang, and S. Fan, Violating Kirchhoff's law of thermal radiation in semitransparent structures, *ACS Photon.* **8**, 2417 (2021).
- [26] L. Zhu, A. Fiorino, D. Thompson, R. Mittapally, E. Meyhofer, and P. Reddy, Near-field photonic cooling through control of the chemical potential of photons, *Nature (London)* **566**, 239 (2019).
- [27] T. Li, Y. Zhai, S. He, W. Gan, Z. Wei, M. Heidarnejad, D. Dalgo, R. Mi, X. Zhao, J. Song, J. Dai, C. Chen, A. Aili, A. Vellore, A. Martini, R. Yang, J. Srebric, X. Yin, and L. Hu, A radiative cooling structural material, *Science* **364**, 760 (2019).
- [28] Y. Li, W. Li, T. Han, X. Zheng, J. Li, B. Li, S. Fan, and C.-W. Qiu, Transforming heat transfer with thermal metamaterials and devices, *Nat. Rev. Mater.* **6**, 488 (2021).
- [29] T. Liu, C. Guo, W. Li, and S. Fan, Thermal photonics with broken symmetries, *eLight* **2**, 25 (2022).
- [30] C. Guo, B. Zhao, and S. Fan, Adjoint Kirchhoff's law and general symmetry implications for all thermal emitters, *Phys. Rev. X* **12**, 021023 (2022).
- [31] C. Guo and S. Fan, Majorization theory for unitary control of optical absorption and emission, *Phys. Rev. Lett.* **130**, 146202 (2023).
- [32] D. A. B. Miller, Self-configuring universal linear optical component [Invited], *Photon. Res.* **1**, 1 (2013).
- [33] J. Carolan, C. Harrold, C. Sparrow, E. Martín-López, N. J. Russell, J. W. Silverstone, P. J. Shadbolt, N. Matsuda, M. Oguma, M. Itoh, G. D. Marshall, M. G. Thompson, J. C. F. Matthews, T. Hashimoto, J. L. O'Brien, and A. Laing, Universal linear optics, *Science* **349**, 711 (2015).
- [34] Y. Shen, N. C. Harris, S. Skirlo, M. Prabhu, T. Baehr-Jones, M. Hochberg, X. Sun, S. Zhao, H. Larochelle, D. Englund, and M. Soljačić, Deep learning with coherent nanophotonic circuits, *Nat. Photon.* **11**, 441 (2017).
- [35] T. Zhu, C. Guo, J. Huang, H. Wang, M. Orenstein, Z. Ruan, and S. Fan, Topological optical differentiator, *Nat. Commun.* **12**, 680 (2021).
- [36] O. Y. Long, C. Guo, H. Wang, and S. Fan, Isotropic topological second-order spatial differentiator operating in transmission mode, *Opt. Lett.* **46**, 3247 (2021).
- [37] S. M. Popoff, A. Goetschy, S. F. Liew, A. D. Stone, and H. Cao, Coherent control of total transmission of light through disordered media, *Phys. Rev. Lett.* **112**, 133903 (2014).
- [38] S. F. Liew, S. M. Popoff, S. W. Sheehan, A. Goetschy, C. A. Schmuttenmaer, A. D. Stone, and H. Cao, Coherent control of photocurrent in a strongly scattering photoelectrochemical system, *ACS Photon.* **3**, 449 (2016).
- [39] M. Mounaix, D. Andreoli, H. Defienne, G. Volpe, O. Katz, S. Grésillon, and S. Gigan, Spatiotemporal coherent control of light through a multiple scattering medium with the multispectral transmission Matrix, *Phys. Rev. Lett.* **116**, 253901 (2016).
- [40] Y. D. Chong, L. Ge, H. Cao, and A. D. Stone, Coherent perfect absorbers: Time-reversed lasers, *Phys. Rev. Lett.* **105**, 053901 (2010).
- [41] W. Wan, Y. Chong, L. Ge, H. Noh, A. D. Stone, and H. Cao, Time-reversed lasing and interferometric control of absorption, *Science* **331**, 889 (2011).
- [42] Y. Sun, W. Tan, H.-q. Li, J. Li, and H. Chen, Experimental demonstration of a coherent perfect absorber with PT phase transition, *Phys. Rev. Lett.* **112**, 143903 (2014).
- [43] D. G. Baranov, A. Krasnok, T. Shegai, A. Alù, and Y. Chong, Coherent perfect absorbers: Linear control of light with light, *Nat. Rev. Mater.* **2**, 17064 (2017).
- [44] A. Müllers, B. Santra, C. Baals, J. Jiang, J. Benary, R. Labouvie, D. A. Zezyulin, V. V. Konotop, and H. Ott, Coherent perfect absorption of nonlinear matter waves, *Sci. Adv.* **4**, eaat6539 (2018).
- [45] K. Pichler, M. Kühmayer, J. Böhm, A. Brandstötter, P. Ambichl, U. Kuhl, and S. Rotter, Random anti-lasing through coherent perfect absorption in a disordered medium, *Nature (London)* **567**, 351 (2019).
- [46] W. R. Sweeney, C. W. Hsu, S. Rotter, and A. D. Stone, Perfectly absorbing exceptional points and chiral absorbers, *Phys. Rev. Lett.* **122**, 093901 (2019).
- [47] L. Chen, T. Kottos, and S. M. Anlage, Perfect absorption in complex scattering systems with or without hidden symmetries, *Nat. Commun.* **11**, 5826 (2020).
- [48] C. Wang, W. R. Sweeney, A. D. Stone, and L. Yang, Coherent perfect absorption at an exceptional point, *Science* **373**, 1261 (2021).
- [49] Y. Slobodkin, G. Weinberg, H. Hörner, K. Pichler, S. Rotter, and O. Katz, Massively degenerate coherent perfect absorber for arbitrary wavefronts, *Science* **377**, 995 (2022).
- [50] A. Krasnok, D. Baranov, H. Li, M.-A. Miri, F. Monticone, and A. Alù, Anomalies in light scattering, *Adv. Opt. Photon.* **11**, 892 (2019).
- [51] X. Ni, S. Yves, A. Krasnok, and A. Alù, Topological metamaterials, *Chem. Rev.* **123**, 7585 (2023).
- [52] C. Guo, J. Li, M. Xiao, and S. Fan, Singular topology of scattering matrices, *Phys. Rev. B* **108**, 155418 (2023).
- [53] S. Longhi, Coherent virtual absorption for discretized light, *Opt. Lett.* **43**, 2122 (2018).

- [54] G. Trainiti, Y. Ra'di, M. Ruzzene, and A. Alù, Coherent virtual absorption of elastodynamic waves, *Sci. Adv.* **5**, eaaw3255 (2019).
- [55] Q. Zhong, L. Simonson, T. Kottos, and R. El-Ganainy, Coherent virtual absorption of light in microring resonators, *Phys. Rev. Res.* **2**, 013362 (2020).
- [56] W. R. Sweeney, C. W. Hsu, and A. D. Stone, Theory of reflectionless scattering modes, *Phys. Rev. A* **102**, 063511 (2020).
- [57] A. D. Stone, W. R. Sweeney, C. W. Hsu, K. Wisal, and Z. Wang, Reflectionless excitation of arbitrary photonic structures: A general theory, *Nanophotonics* **10**, 343 (2021).
- [58] M. Horodynski, M. Kühmayer, C. Ferise, S. Rotter, and M. Davy, Anti-reflection structure for perfect transmission through complex media, *Nature (London)* **607**, 281 (2022).
- [59] J. Sol, A. Alhulaymi, A. D. Stone, and P. del Hougne, Reflectionless programmable signal routers, *Sci. Adv.* **9**, eadf0323 (2023).
- [60] C. F. Bohren and D. R. Huffman, *Absorption and Scattering of Light by Small Particles* (Wiley-VCH, Weinheim, 2004).
- [61] J. R. Taylor, *Scattering Theory: The Quantum Theory of Nonrelativistic Collisions* (Dover Publications, Mineola, NY, 2006).
- [62] The scattering coefficient is defined as  $\chi_s = |\beta|^2 = \chi_e - \chi_a$ .
- [63] P. Ambichl, A. Brandstötter, J. Böhm, M. Kühmayer, U. Kuhl, and S. Rotter, Focusing inside disordered media with the generalized Wigner-Smith operator, *Phys. Rev. Lett.* **119**, 033903 (2017).
- [64] S. Rotter and S. Gigan, Light fields in complex media: Mesoscopic scattering meets wave control, *Rev. Mod. Phys.* **89**, 015005 (2017).
- [65] H. Cao, A. P. Mosk, and S. Rotter, Shaping the propagation of light in complex media, *Nat. Phys.* **18**, 994 (2022).
- [66] The compression of a linear operator  $\hat{O}$  on a Hilbert space  $H$  to a subspace  $H_i$  is the operator  $\hat{P}\hat{O} : H_i \rightarrow H_i$ , where  $\hat{P}$  is the projection from  $H$  to  $H_i$  [131,132].
- [67] H.-H. Perkampus, *UV-VIS Spectroscopy and its Applications* (Springer Berlin Heidelberg, Berlin, Heidelberg, 1992).
- [68] G. G. Hammes, *Spectroscopy for the Biological Sciences* (John Wiley & Sons, 2005).
- [69] W. W. Parson, *Modern Optical Spectroscopy* (Springer Berlin Heidelberg, New York, NY, 2015).
- [70] M. A. Linne, *Spectroscopic Measurement: An Introduction to the Fundamentals* (Elsevier, New York, 2024).
- [71] L. Hoff, *Acoustic Characterization of Contrast Agents for Medical Ultrasound Imaging* (Springer Netherlands, Dordrecht, 2001).
- [72] U. Platt and J. Stutz, *Differential Optical Absorption Spectroscopy*, Physics of Earth and Space Environments (Springer Berlin Heidelberg, Berlin, Heidelberg, 2008).
- [73] K. N. Rao, *Spectroscopy of the Earth's Atmosphere and Interstellar Medium* (Academic Press, New York, 2012).
- [74] J. Tennyson, *Astronomical Spectroscopy: An Introduction to the Atomic and Molecular Physics of Astronomical Spectroscopy*, 3rd ed., Advanced Textbooks in Physics (World Scientific, Europe, 2019).
- [75] K. O. Hill, B. Malo, K. Vineberg, F. Bilodeau, D. C. Johnson, and I. Skinner, Efficient mode conversion in telecommunication fiber using externally written gratings, in *Optical Society of America Annual Meeting (1990)*, Paper TuRR2 (Optica Publishing Group, 1990), p. TuRR2.
- [76] K. S. Lee and T. Erdogan, Fiber mode conversion with tilted gratings in an optical fiber, *J. Opt. Soc. Am. A* **18**, 1176 (2001).
- [77] D. A. B. Miller, All linear optical devices are mode converters, *Opt. Express* **20**, 23985 (2012).
- [78] J. Lu and J. Vučković, Objective-first design of high-efficiency, small-footprint couplers between arbitrary nanophotonic waveguide modes, *Opt. Express* **20**, 7221 (2012).
- [79] J. Wang, J.-Y. Yang, I. M. Fazal, N. Ahmed, Y. Yan, H. Huang, Y. Ren, Y. Yue, S. Dolinar, M. Tur, and A. E. Willner, Terabit free-space data transmission employing orbital angular momentum multiplexing, *Nat. Photon.* **6**, 488 (2012).
- [80] M. Heinrich, M.-A. Miri, S. Stützer, R. El-Ganainy, S. Nolte, A. Szameit, and D. N. Christodoulides, Supersymmetric mode converters, *Nat. Commun.* **5**, 3698 (2014).
- [81] D. Ohana and U. Levy, Mode conversion based on dielectric metamaterial in silicon, *Opt. Express* **22**, 27617 (2014).
- [82] Y. Zhao, Y. Liu, L. Zhang, C. Zhang, J. Wen, and T. Wang, Mode converter based on the long-period fiber gratings written in the two-mode fiber, *Opt. Express* **24**, 6186 (2016).
- [83] Z. Huan, R. Scarmozzino, G. Nagy, J. Steel, and R. Osgood, Realization of a compact and single-mode optical passive polarization converter, *IEEE Photon. Technol. Lett.* **12**, 317 (2000).
- [84] Y. Guo, M. Xiao, and S. Fan, Topologically protected complete polarization conversion, *Phys. Rev. Lett.* **119**, 167401 (2017).
- [85] Y. Guo, M. Xiao, Y. Zhou, and S. Fan, Arbitrary polarization conversion with a photonic crystal slab, *Adv. Opt. Mater.* **7**, 1801453 (2019).
- [86] C. Guo, M. Xiao, Y. Guo, L. Yuan, and S. Fan, Meron spin textures in momentum space, *Phys. Rev. Lett.* **124**, 106103 (2020).
- [87] J. C. Gutiérrez-Vega, The field of values of Jones matrices: Classification and special cases, *Proc. R. Soc. Ser. A* **476**, 20200361 (2020).
- [88] Y. Zeng, G. Hu, K. Liu, Z. Tang, and C.-W. Qiu, Dynamics of topological polarization singularity in momentum space, *Phys. Rev. Lett.* **127**, 176101 (2021).
- [89] W. Liu, W. Liu, L. Shi, and Y. Kivshar, Topological polarization singularities in metaphotonics, *Nanophotonics* **10**, 1469 (2021).
- [90] S. Biswas, M. Y. Grajower, K. Watanabe, T. Taniguchi, and H. A. Atwater, Broadband electro-optic polarization conversion with atomically thin black phosphorus, *Science* **374**, 448 (2021).
- [91] A. H. Dorrah, N. A. Rubin, A. Zaidi, M. Tamagnone, and F. Capasso, Metasurface optics for on-demand polarization transformations along the optical path, *Nat. Photon.* **15**, 287 (2021).
- [92] C. He, H. He, J. Chang, B. Chen, H. Ma, and M. J. Booth, Polarisation optics for biomedical and clinical applications: A review, *Light Sci. Appl.* **10**, 194 (2021).
- [93] Z. Y. Li, S. J. Li, B. W. Han, G. S. Huang, Z. X. Guo, and X. Y. Cao, Quad-band transmissive metasurface with linear to dual-circular polarization conversion simultaneously, *Adv. Theory Simul.* **4**, 2100117 (2021).
- [94] H. Li, C. Zheng, H. Xu, J. Li, C. Song, J. Li, L. Wu, F. Yang, Y. Zhang, W. Shi, and J. Yao, Diatomic terahertz metasurfaces for arbitrary-to-circular polarization conversion, *Nanoscale* **14**, 12856 (2022).

- [95] M. Kang, Z. Zhang, T. Wu, X. Zhang, Q. Xu, A. Krasnok, J. Han, and A. Alù, Coherent full polarization control based on bound states in the continuum, *Nat. Commun.* **13**, 4536 (2022).
- [96] S.-H. Kim, R. Takei, Y. Shoji, and T. Mizumoto, Single-trench waveguide TE-TM mode converter, *Opt. Express* **17**, 11267 (2009).
- [97] S. Li, Q. Mo, X. Hu, C. Du, and J. Wang, Controllable all-fiber orbital angular momentum mode converter, *Opt. Lett.* **40**, 4376 (2015).
- [98] C. Fu, S. Liu, Z. Bai, J. He, C. Liao, Y. Wang, Z. Li, Y. Zhang, K. Yang, B. Yu, and Y. Wang, Orbital angular momentum mode converter based on helical long period fiber grating inscribed by hydrogen–oxygen flame, *J. Lightwave Technol.* **36**, 1683 (2018).
- [99] P. S. Vukusic, G. P. Bryan-Brown, and J. R. Sambles, Surface plasmon resonance on gratings as a novel means for gas sensing, *Sens. Actuators, B* **8**, 155 (1992).
- [100] B. Gu, W. Qi, Y. Zhou, Z. Wu, P. P. Shum, and F. Luan, Reflective liquid level sensor based on modes conversion in thin-core fiber incorporating tilted fiber Bragg grating, *Opt. Express* **22**, 11834 (2014).
- [101] R. Verre, N. Maccaferri, K. Fleischer, M. Svedendahl, N. O. Länk, A. Dmitriev, P. Vavassori, I. V. Shvets, and M. Käll, Polarization conversion-based molecular sensing using anisotropic plasmonic metasurfaces, *Nanoscale* **8**, 10576 (2016).
- [102] H. Zhang, Y. Liu, Z. Liu, X. Liu, G. Liu, G. Fu, J. Wang, and Y. Shen, Multi-functional polarization conversion manipulation via graphene-based metasurface reflectors, *Opt. Express* **29**, 70 (2021).
- [103] Z. Zhang, C. Zhong, F. Fan, G. Liu, and S. Chang, Terahertz polarization and chirality sensing for amino acid solution based on chiral metasurface sensor, *Sens. Actuators, B* **330**, 129315 (2021).
- [104] G. B. Xavier, G. V. de Faria, G. P. Temporão, and J. P. von der Weid, Full polarization control for fiber optical quantum communication systems using polarization encoding, *Opt. Express* **16**, 1867 (2008).
- [105] A. Mohanty, M. Zhang, A. Dutt, S. Ramelow, P. Nussenzveig, and M. Lipson, Quantum interference between transverse spatial waveguide modes, *Nat. Commun.* **8**, 14010 (2017).
- [106] C. Fabre and N. Treps, Modes and states in quantum optics, *Rev. Mod. Phys.* **92**, 035005 (2020).
- [107] Z. Liang, J. Li, and Y. Wu, All-optical polarization-state engineering in quantum cavity optomagnonics, *Phys. Rev. A* **107**, 033701 (2023).
- [108] C. Guo, Y. Guo, and S. Fan, Relation between photon thermal Hall effect and persistent heat current in nonreciprocal radiative heat transfer, *Phys. Rev. B* **100**, 205416 (2019).
- [109] R. A. Horn and C. R. Johnson, *Topics in Matrix Analysis* (Cambridge University Press, Cambridge, 2008).
- [110] K. E. Gustafson and D. K. M. Rao, *Numerical Range: The Field of Values of Linear Operators and Matrices*, Universitext (Springer, New York, 1997).
- [111] O. Toeplitz, Das algebraische Analogon zu einem Satze von Fejér, *Math. Z.* **2**, 187 (1918).
- [112] F. Hausdorff, Der Wertvorrat einer Bilinearform, *Math. Z.* **3**, 314 (1919).
- [113] See Supplemental Material at <http://link.aps.org/supplemental/10.1103/PhysRevA.109.L061503> for numerical range, examples of scattering submatrices, Kato's theorem, matrix determinant lemma, proof of Eq. (27), topological phases of a resonance, and additional numerical results, which includes Refs. [133–147].
- [114] C. R. Crawford, A stable generalized eigenvalue problem, *SIAM J. Numer. Anal.* **13**, 854 (1976).
- [115] K.-Z. Wang, P. Y. Wu, and H.-L. Gau, Crawford numbers of powers of a matrix, *Linear Algebra Appl.* **433**, 2243 (2010).
- [116] G. Choi and H. J. Lee, On the Crawford number attaining operators, *Rev. Mat. Complutense* **36**, 841 (2023).
- [117] P. J. Psarrakos and M. J. Tsatsomeros, Numerical Range (In) a Matrix Nutshell, Lecture notes, Department of Mathematics, Washington State University **1**, 1 (2002).
- [118] X. H. Wu, J. J. Huang, and Alatancang, On the origin and numerical range of bounded operators, *Acta Math. Sin., English Series* **35**, 1715 (2019).
- [119] This difference arises because coherent orthogonal scattering, as defined by a system of quadratic equations [Eq. (8)], is more complicated than coherent perfect extinction, as defined by a system of linear equations [Eq. (9)].
- [120] J. Roe, *Winding Around: The Winding Number in Topology, Geometry, and Analysis*, Student Mathematical Library Vol. 76 (American Mathematical Society, Providence, RI, 2015).
- [121] W. A. Stein, *Elementary Number Theory: Primes, Congruences, and Secrets: A Computational Approach*, Undergraduate Texts in Mathematics (Springer, New York, NY, 2009).
- [122] I. M. Spitkovsky, Stability of partial indices of a Riemann boundary-value problem with a strictly nonsingular matrix, *Doklady Akademii Nauk SSSR* **218**, 46 (1974).
- [123] C. Guo and S. Fan, Winding number criterion for the origin to belong to the numerical range of a matrix on a loop of matrices, [arXiv:2311.00849](https://arxiv.org/abs/2311.00849).
- [124] T. Kato, *Perturbation Theory for Linear Operators*, Classics in Mathematics (Springer, Berlin, 1995).
- [125] C.-K. Li and F. Zhang, Eigenvalue continuity and Gershgorin's theorem, *Electron. J. Linear Alg.* **35**, 619 (2019).
- [126] H. A. Haus, *Waves and Fields in Optoelectronics*, Prentice-Hall Series in Solid State Physical Electronics (Prentice-Hall, Englewood Cliffs, NJ, 1984).
- [127] S. Fan, W. Suh, and J. D. Joannopoulos, Temporal coupled-mode theory for the Fano resonance in optical resonators, *J. Opt. Soc. Am. A* **20**, 569 (2003).
- [128] W. Suh, Z. Wang, and S. Fan, Temporal coupled-mode theory and the presence of non-orthogonal modes in lossless multimode cavities, *IEEE J. Quantum Electron.* **40**, 1511 (2004).
- [129] H. Zhou, B. Zhen, C. W. Hsu, O. D. Miller, S. G. Johnson, J. D. Joannopoulos, and M. Soljačić, Perfect single-sided radiation and absorption without mirrors, *Optica* **3**, 1079 (2016).
- [130] S. Fan and J. D. Joannopoulos, Analysis of guided resonances in photonic crystal slabs, *Phys. Rev. B* **65**, 235112 (2002).
- [131] P. R. Halmos, *A Hilbert Space Problem Book*, 2nd ed., Graduate Texts in Mathematics No. 19 (Springer-Verlag, New York, 1982).
- [132] V. I. Istratescu, *Introduction to Linear Operator Theory* (CRC Press, Boca Raton, FL, 2020).
- [133] J. R. Munkres, *Topology*, 2nd ed. (Prentice Hall, Inc., Upper Saddle River, NJ, 2000).

- [134] R. Kippenhahn, Über den Wertevorrat einer Matrix, *Math. Nachr.* **6**, 193 (1951).
- [135] P. F. Zachlin and M. Hochstenbach, On the numerical range of a matrix [Translation of R. Kippenhahn (1951), Über den Wertevorrat einer Matrix, *Mathematische Nachrichten* 6, 193–228], *Linear Multilinear Algebra* **56**, 185 (2008).
- [136] J. W. Helton and V. Vinnikov, Linear matrix inequality representation of sets, *Commun. Pure Appl. Math.* **60**, 654 (2007).
- [137] D. Henrion, Semidefinite geometry of the numerical range, *Electron. J. Linear Alg.* **20**, 322 (2010).
- [138] J. W. Helton and I. M. Spitkovsky, The possible shapes of numerical ranges, *Operators and Matrices* **6**, 607 (2012).
- [139] D. S. Keeler, L. Rodman, and I. M. Spitkovsky, The numerical range of  $3 \times 3$  matrices, *Linear Alg. Appl.* **252**, 115 (1997).
- [140] E. S. Brown and I. M. Spitkovsky, On matrices with elliptical numerical ranges, *Linear Multilinear Alg.* **52**, 177 (2004).
- [141] H.-L. Gau, Elliptic numerical ranges of  $4 \times 4$  matrices, *Taiwan. J. Math.* **10**, 117 (2006).
- [142] E. Militzer, L. J. Patton, I. M. Spitkovsky, and M.-C. Tsai, Numerical ranges of 4-by-4 nilpotent matrices: Flat portions on the boundary, in *Large Truncated Toeplitz Matrices, Toeplitz Operators, and Related Topics: The Albrecht Böttcher Anniversary Volume*, Operator Theory: Advances and Applications, edited by D. A. Bini, T. Ehrhardt, A. Y. Karlovich, and I. Spitkovsky (Springer International Publishing, Cham, 2017), pp. 561–591.
- [143] M. Cox, W. Grewe, G. Hochrein, L. Patton, and I. Spitkovsky, Nonparallel flat portions on the boundaries of numerical ranges of 4-by-4 nilpotent matrices, *Electron. J. Linear Algebra* **37**, 504 (2021).
- [144] T. Geryba and I. M. Spitkovsky, On some 4-by-4 matrices with bi-elliptical numerical ranges, *Linear Multilin. Alg.* **69**, 855 (2021).
- [145] C. D. Meyer, *Matrix Analysis and Applied Linear Algebra* (Society for Industrial and Applied Mathematics, Philadelphia, PA, 2000).
- [146] T. Needham, *Visual Differential Geometry and Forms: A Mathematical Drama in Five Acts* (Princeton University Press, Princeton, NJ, 2021).
- [147] Z. Zhao, C. Guo, and S. Fan, Connection of temporal coupled-mode-theory formalisms for a resonant optical system and its time-reversal conjugate, *Phys. Rev. A* **99**, 033839 (2019).